Materials Science and Engineering C 61 (2016) 832–841

Contents lists available at ScienceDirect

Materials Science and Engineering C

journal homepage: www.elsevier.com/locate/msec

Layer-by-layer films containing peptides of the Cry1Ab16 toxin from *Bacillus thuringiensis* for potential biotechnological applications

Alexandra Plácido [a], Emanuel Airton de Oliveira Farias [b], Mariela M. Marani [c], Andreanne G. Vasconcelos [b], Ana C. Mafud [d], Yvonne P. Mascarenhas [d], Carla Eiras [b,e], José R.S.A. Leite [b,*], Cristina Delerue-Matos [a]

[a] REQUIMTE/LAQV, Instituto Superior de Engenharia do Porto, Instituto Politécnico do Porto, Rua Dr. António Bernardino de Almeida, 431, 4200-072 Porto, Portugal
[b] Núcleo de Pesquisa em Biodiversidade e Biotecnologia, BIOTEC, Campus Ministro Reis Velloso, CMRV, Universidade Federal do Piauí, UFPI, 64202020 Parnaíba, Piaui, Brazil
[c] IPEEC-CENPAT-CONICET, Centro Nacional Patagónico, Consejo Nacional de Investigaciones Científicas y Técnicas, 9120 Puerto Madryn, Chubut, Argentina
[d] Instituto de Física de São Carlos, Universidade de São Paulo, USP, 13566-590 São Carlos, SP, Brazil
[e] Laboratório de Materiais Avançados, LIMAV, Engenharia de Materiais, Centro de Tecnologia, CT, Universidade Federal do Piauí, UFPI, 64049550 Teresina, Piaui, Brazil

ARTICLE INFO

Article history:
Received 19 October 2015
Received in revised form 26 November 2015
Accepted 4 January 2016
Available online 9 January 2016

Keywords:
Cry1Ab16 toxin
Genetically modified organism
Layer-by-layer film
Bioelectrochemistry

ABSTRACT

Cry1Ab16 is a toxin of crystalline insecticidal proteins that has been widely used in genetically modified organisms (GMOs) to gain resistance to pests. For the first time, in this study, peptides derived from the immunogenic Cry1Ab16 toxin (from *Bacillus thuringiensis*) were immobilized as layer-by-layer (LbL) films. Given the concern about food and environmental safety, a peptide with immunogenic potential, PcL342–354C, was selected for characterization of the electrochemical, optical, and morphological properties. The results obtained by cyclic voltammetry (CV) showed that the peptide have an irreversible oxidation process in electrolyte of 0.1 mol·L^{-1} potassium phosphate buffer (PBS) at pH 7.2. It was also observed that the electrochemical response of the peptide is governed mainly by charge transfer. In an attempt to maximize the electrochemical signal of peptide, it was intercalated with natural (agar, alginate and chitosan) or synthetic polymers (polyethylenimine (PEI) and poly(sodium 4-styrenesulfonate (PSS)). The presence of synthetic polymers on the film increased the electrochemical signal of PcL342–354C up to 100 times. Images by Atomic Force Microscopy (AFM) showed that the immobilized PcL342–354C formed self-assembled nanofibers with diameters ranging from 100 to 200 nm on the polymeric film. By UV–Visible spectroscopy (UV–Vis) it was observed that the ITO/PEI/PSS/PcL342–354C film grows linearly up to the fifth layer, thereafter tending to saturation. X-ray diffraction confirmed the presence on the films of crystalline ITO and amorphous polypeptide phases. In general, the ITO/PEI/PSS/PcL342–354C film characterization proved that this system is an excellent candidate for applications in electrochemical sensors and other biotechnological applications for GMOs and environmental indicators.

1. Introduction

Nanotechnology of thin films is a multidisciplinary science that has attracted attention around the world owing to the impact that these films can have in the technology sector [1–3]. Among the thin film production techniques, layer-by-layer (LbL) self-assembly stands out because of its versatility, which has enabled applications in the fields of biomaterials, biosensors, drug/gene delivery, tissue engineering, implantable materials, diagnostics, electronics, energy, and optics [4–6].

The self-assembly process is characterized by the absence of an external or human influence, as the system takes the most appropriate conformation according to thermodynamic factors [7]. This configuration is due to the various molecular interactions that can occur between materials when interleaved as LbL films. Electrostatic, hydrophobic, charge transfer, hydrogen bonding, and covalent interactions, as well as Van der Waals forces, are examples of interactions that may occur in self-assembled LbL films [8].

The versatility of the LbL technique has enabled the development of various devices using a variety of materials, such as proteins [9–12], conductive polymers [13–15] polysaccharides [14,16,17], and dyes [18]. Furthermore, LbL peptide-based films were developed for applications in sensors for thrombin and other proteins of biological interest [19]. Peptides have also been used in the composition of LbL films for applications as sensors of heparin [20], vancomycin [21], and other drugs, or the detection of gas [22]. Another interesting example is the use of peptide AVPFAQKG to make a sensor capable of directly detecting the BIR3 domain, which is a protein-linked inhibitor of apoptosis (XIAP-BIR3) [23]. There are also reports using fluorescent peptides to detect "*tyrosine sulfurylation*", which is an important post-translational modification of protein–protein interactions in the extracellular space that is crucial in cell adhesion, cell signaling, immune response, and recognition of pathogens in host cells [24,25].

* Corresponding author.
E-mail addresses: jrsaleite@gmail.com, jrleite@cnpq.br (J.R.S.A. Leite).

http://dx.doi.org/10.1016/j.msec.2016.01.011
0928-4931/

Our research group has pioneered the use of peptides to manufacture biodevices to demonstrate the LbL immobilization of a bioactive peptide (Dermaseptin 01, DRS-01) for antileishmanial activity assays. We use an electrochemical biosensor to detect lysing of the membrane of living cells of *Leishmania infantum* promoted by the action of the immobilized peptide [26] Clearly, peptides are potential candidates to meet the needs of the modern world in relation to diagnosis, disease monitoring, quality control in industry, and more recently, detection of genetically modified organisms (GMOs) and food security through the development of biosensors [27]. In this sense, our group has developed immunogenic peptides derived from the 5-enolpyruvylshikimate-3-phosphate synthase (CP4-EPSPS) from *Agrobacterium tumefaciens* with in silico prediction [28] based on the structural features of the enzyme, aiming at further development of antibodies for use in sensors for the detection of GMOs or environmental sensors. CP4-EPSPS is an enzyme that decreases the binding affinity to glyphosate, conferring increased tolerance to the glyphosate herbicide that has been widely used in GMOs to gain resistance to pests [28].

Concern about food safety and the environment has stimulated interest in establishing sensitive means to detect GMO. An important group of proteins is insecticidal crystal proteins (ICPs) such as Cry1Ab toxin. Cry1Ab is a toxin from *Bacillus thuringiensis* that was incorporated to GMO maize to confer resistance to the European corn borer (*Ostrinia nubilalis*). This toxin was detected in maternal and fetal samples during pesticide exposure studies associated with genetically modified foods [29]. In addition, the effect of genetically modified crops on ecosystems has been a focus of environmental risk assessment studies, considering that insecticidal proteins, such as Cry1Ab, can pass into the aquatic environment [30].

Therefore, the aim of this work was the immobilization of the PcL342–354C peptide, derived from the Cry1Ab protein, in the form of LbL films for future applications in GMO sensors. Previously four peptides from the Cry1Ab protein were selected through in silico analysis; after studies of the solubility in aqueous media and the structural characteristics determined by circular dichroism, the PcL342–354C peptide was chosen for further study of new materials and nanodevices. Initially, film construction was studied to analyze the peptide immobilization conditions and electrochemical behavior. Subsequently, LbL films of this peptide interspersed with natural or synthetic polymers were constructed with the aim of amplifying the electrochemical signal of the peptide for the development of new materials and future biosensors. Finally, the system was characterized using various morphological and spectroscopic techniques such as Atomic Force Microscopy (AFM), UV–Vis, X-ray diffraction (XRD), and Fourier Transform Infrared Spectroscopy (FTIR). The system proposed here proved to be feasible and relevant for future applications in GMO sensors and other biotechnological applications.

2. Materials and methods

2.1. Peptide synthesis

Cry1Ab16 protein sequence was retrieved from the NCBI database (access number AAK55546) (Fig. 1A). Peptides were selected by in silico evaluation based on their sequence and immunogenicity. Peptides were manually synthesized using a solid phase approach with Fmoc/t-butyl chemistry [31]. Peptide elongation was carried out in polypropylene syringes fitted with a polyethylene porous disk. Solvents and soluble reagents were removed by suction. A Rink amide MBHA resin (Peptides International) was used for the synthesis of the peptides. A Cys residue was incorporated at the C-terminus to allow subsequent coupling. Samples were treated with trifluoroacetic acid/triisopropylsilane/water (TFA/TIS/H_2O) (95:2.5:2.5) to remove the protecting groups. Peptide purification was carried out using an analytical RP-HPLC system (Shimadzu Prominence instrument, Shimadzu Co.) equipped with a reverse-phase (RP) chromatographic column (Kinetex 5 μm C_{18}, 50 × 21.20 mm, Phenomenex). Each peptide was dissolved in H_2O:CH_3CN (6:4) and subjected to RP-HPLC using a gradient of CH_3CN, starting with H_2O (0.1% TFA) and increasing to 100% CH_3CN over 60 min at a flow rate of 1.0 mL/min. The peptides were monitored at 216 and 280 nm. The formula $(A_{215} - A_{225}) \times 144$ (μg/mL) was applied for peptide quantification [32]. Purity and molecular mass determination of the synthetic peptides were performed using a MALDI-TOF/TOF mass spectrometer (UltrafleXtreme, Bruker Daltonics) [33].

2.2. Far-UV circular dichroism

To estimate the secondary structure of the peptides, far-ultraviolet circular dichroism (far-UV CD) spectroscopy was carried out. The absorbance of circularly polarized light was measured in different

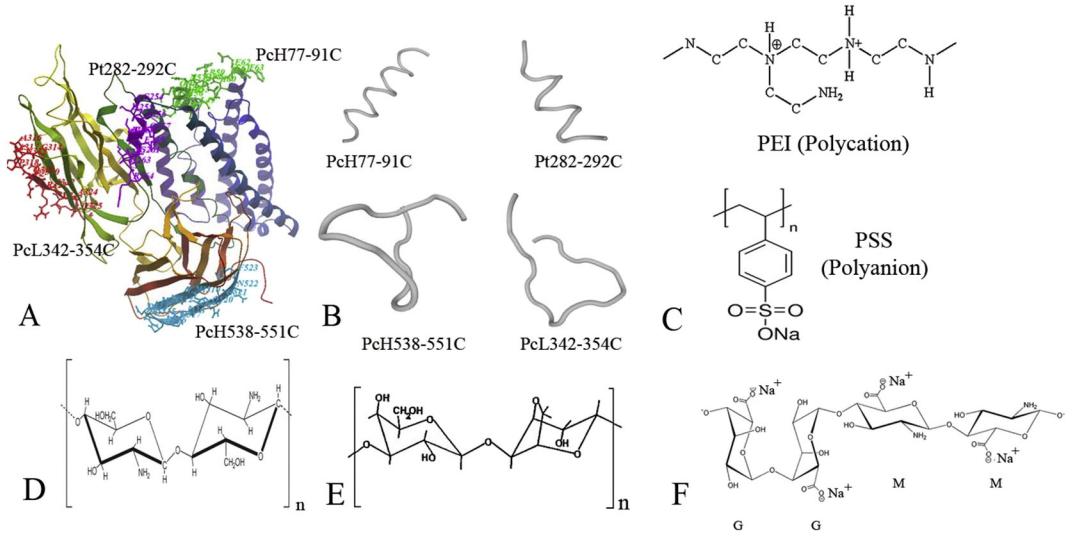

Fig. 1. (A) 3-D structure of the Cry1Ab16 protein obtained by homology modeling [61], showing the location of the four peptides selected in the study. (B) PDB secondary structure models were obtained using the Web resource PEP-FOLD (http://bioserv.rpbs.univparis-diderot.fr/cgi-bin/PEP-FOLD). The peptides were synthesized with a C-terminal cysteine for subsequent coupling to a carrier protein for antibody production feasibility and/or coupled nanoparticles for other applications. (C) Polyelectrolytes: polycation (PEI, polyethylenimine) and polyanion (PSS, poly(sodium 4-styrenesulfonate). (D) Chitosan (D-glucosamine and *N*-acetylglucosamine monomers). (E) Agar (β-(1-3)-D and α-(1-4)-L linked galactose residues). (F) Sodium alginate (alginic acid is a linear copolymer with homopolymeric blocks of (1-4)-linked β-D-mannuronate (M) and the C-5 epimer of α-L-guluronate (G) residues).

peptide solutions. The analysis of the CD data is based on a basic principle: the CD spectrum can be expressed as a linear combination of the spectra of the individual secondary structure components. The parameters were obtained using three of the most popular methods: CONTIN/LL [34], SELCON3 [35] and CDSSTR [36]. Far-UV CD spectra were obtained using a JASCO J 815 spectropolarimeter. The measurements were performed under a nitrogen gas flow of 8 L/h at a temperature of 20 °C, which was controlled by a Peltier system (JASCO). The spectra were recorded between 190 and 240 nm, using a 100 mm cell path length. The peptides were dissolved in Milli-Q water at a concentration of 100 μM with various concentrations of 2,2,2-trifluoroethanol (TFE). The scan speed was 50 nm/min, the response time was 1 s, and the bandwidth was 1 nm. The spectra were converted to molar ellipticity residue half by using the relationship: $[\Theta] / \Theta(10 \times c \times n \times d)$, where $[\Theta]$ is the molar ellipticity (degrees·cm^2·dmol^{-1}), Θ the ellipticity (millidegrees), n is the number of peptide bonds, c is the molar concentration, and d the length of the cell (cm). The spectra were fitted using the above routines by setting the reference protein to SDP48, which is composed of 48 proteins, 43 soluble and 5 denatured.

2.3. Electrochemical characterization

Electrochemical measurements were performed using an Autolab PGSTAT204 potentiostat/galvanostat and a three-electrode electrochemical cell with a capacity of 10 mL. A platinum plate (area 1.0 cm^2) and silver/silver chloride (Ag/AgCl) were used as the auxiliary and reference electrodes, respectively. LbL films deposited onto indium tin oxide (ITO) (area 1.04 cm^2) were used as the working electrode. All the experiments were performed in ambient atmosphere at 22 °C in an electrolytic solution of 0.05 mol·L^{-1} H_2SO_4 or 0.1 mol·L^{-1} potassium phosphate buffer solution (PBS) (pH 7.2).

2.4. Layer-by-layer film preparation

The LbL films prepared in this work were based on electrostatic interactions between polyelectrolytes, as described by Decher [37]. In an attempt to improve the electrochemical signal of the peptide, it was combined with other polymeric materials in the form of a bilayer film. Chitosan (Fig. 1D) and polyethylenimine (PEI) (Fig. 1C above) were tested as positive polyelectrolytes (polycation), whereas agar (Fig. 1E), alginate (Fig. 1F), and poly(sodium 4-styrenesulfonate (PSS) (Fig. 1C below) were tested as negative polyelectrolytes (polyanion). The preparation process of the films is shown in Fig. 2. Initially, a previously cleaned ITO substrate, which is a ternary composition of indium, tin, and oxygen in varying proportions [38] was immersed in a solution of the polycation or polyanion for 5 min. ITO is one of the most widely used transparent conducting oxides because of its two main properties: electrical conductivity and optical transparency, as well as the ease with which it can be deposited as a thin film. Subsequently, the substrate was washed in ultrapure water to remove the non-adsorbed material, thereby yielding a monolayer film of the polycation or polyanion. Then, the monolayer-modified substrate was immersed in a solution PcL342–354C (Table 1 and Fig. 1B), for 5 min, and then rinsed in ultrapure water. The deposition time was tested and was found to allow a good response in electrochemical systems. Each wash step was preceded by a N_2 drying step.

2.5. Atomic Force Microscopy

Representative films were examined using AFM. The analysis was carried on the samples in vibrating (tapping) mode. Imaging was performed using a TT-AFM instrument (AFM Workshop). All images were collected at 512 pixel resolution for a 4 × 4 μm area, and at least three different areas were examined per sample. Representative data are shown. The images have been processed, analyzed, and displayed using Gwyddion 2.29 software. The roughness values shown are for the 4 × 4 μm areas and represent the roughness average (Ra) values [39].

2.6. Spectroscopic and diffractometric characterization

2.6.1. UV–Vis absorption spectra of LbL films

To record the absorption spectra, LbL films were prepared in a similar manner on an ITO surface. One side of the ITO surface was coated with black paint prior to use to block out incidental light and allow the absorption spectrum of the LbL film located over the aperture to be recorded accurately. The absorption spectra of LbL films were recorded using a UV–Vis absorption spectrophotometer (Evolution 300).

2.6.2. FTIR spectroscopy

The FTIR transmittance spectra were collected using a Shimadzu IRAffinity-1 spectrometer in the spectral range from 3500 to 2500 cm^{-1}.

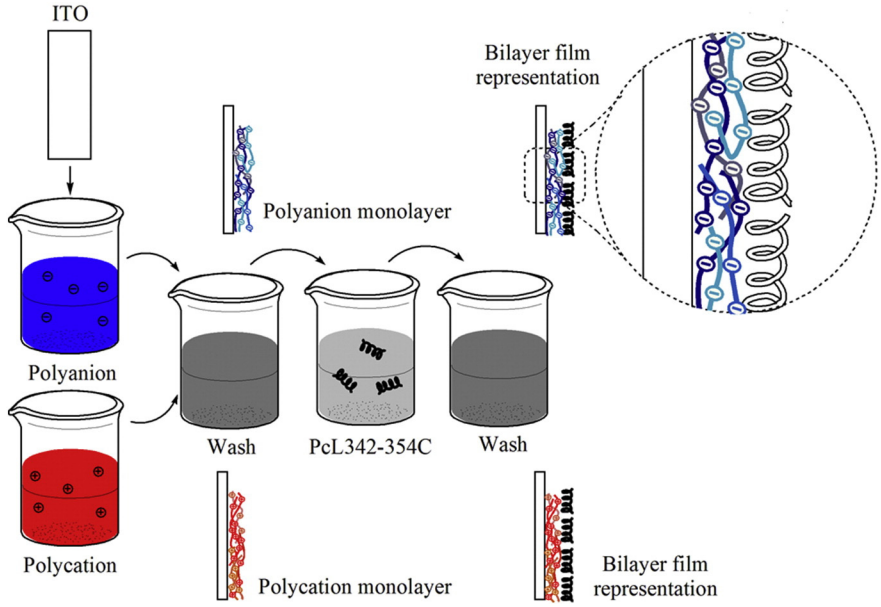

Fig. 2. Illustration of the LbL film deposition process.

Table 1
Chemical and structural characteristics of the peptides used in this work.

Peptide name	Amino acid sequence	Monoisotopic mass	pI[a]	GRAVY[b]
PcH77-91C	LVQIEQLINQRIEEF**C**	1976.30	4.25	0.100
Pt282-292C	GSAQGIEGSIR**C**	1178.35	5.99	−0.083
PcH538-551C	HTSIDGRPINQGNF**C**	1659.82	6.74	0.755
PcL342–354C	GNAAPQQRIVAQL**C**	1469.71	8.25	0.007

[a] Reference [62].
[b] GRand AVerage of hYdropathicity (GRAVY) [63].

2.6.3. X-ray diffraction

XRD data were obtained at the IFSC/USP X-ray crystallography laboratory using a Rigaku Rotaflex diffractometer equipped with a graphite monochromator and rotating anode tube, operating with Cu Kα, 50 kV, and 100 mA. Powder diffraction patterns were obtained in step scanning mode (2θ = 10–60°, step of 0.02°, and 1 s/step). The study of crystalline ITO film phases was obtained by comparison with pure In_2O_3.

3. Results and discussion

3.1. Cry1Ab16 protein and peptide selection

The protein sequence corresponding to Cry1Ab16 (*cry* protein family) was retrieved from the NCBI database (access number AAK55546). Cry1Ab16 is a δ-endotoxin produced by *B. thuringiensis* AC11 (H14). The entire primary sequence of this protein is composed of 1155 amino acids. The ExPASy PeptideCutter tool [40] was used to submit Cry1Ab16 to an in silico cleavage site prediction using trypsin and chymotrypsin for high (HS) and low (LS) specificity.

A cleavage site map and table of cleavage site positions were analyzed and peptides with sequences between 10 and 30 amino acids were selected for compositional analysis. The four selected peptides after theoretical digestion were chosen by considering the antibody production capacity using in silico analysis, such as structure determination of epitopes and T-cell epitope prediction. The solubility in aqueous systems and the prediction of the secondary structure were also used to select the peptide of choice, which is discussed in Section 3.2. The nomenclature of the peptides considers the positioning characteristics of the sequence in the native protein and how the peptide was generated. For example, PcL 342–354C: P = peptide; cL = chymotrypsin LS; 342-354 position in the native protein, and C = cysteine amino residue at the C-terminus (Table 1 and Fig. 1B).

3.2. Far-UV circular dichroism

In biophysics, helicity is closely related to antibacterial activity [41]. Here, we present a secondary structural study for Pt282-292C, PcL342–354C, PcH538-551C, and PcH77-91C in different buffer systems. The results of the CD spectra fitting are shown in Fig. 3. The best fitting of these data was obtained using the CONTIN/LL software, which is plotted for different solutions of these peptides in Fig. 3, with detailed results in Tables S1–S4 in the Supplementary material.

The results showed $[\theta]_{222}$ of PcL342–354C to be -3373.15 degree·cm^2·dmol^{-1} in the presence of 40% TFE to mimic a hydrophobic environment [42], indicating that the peptide formed a typical α-helical fold in hydrophobic environments such as biomembranes (Fig. 3 and Table S1). Using these CD studies and taking into consideration the solubility of the peptides in aqueous media (Table 1, GRAVY index), only the PcL342–354C peptide is further considered in this study for the construction of new materials for biotechnological applications. These characteristics and the size of this sequence can lead to successful production of antibodies.

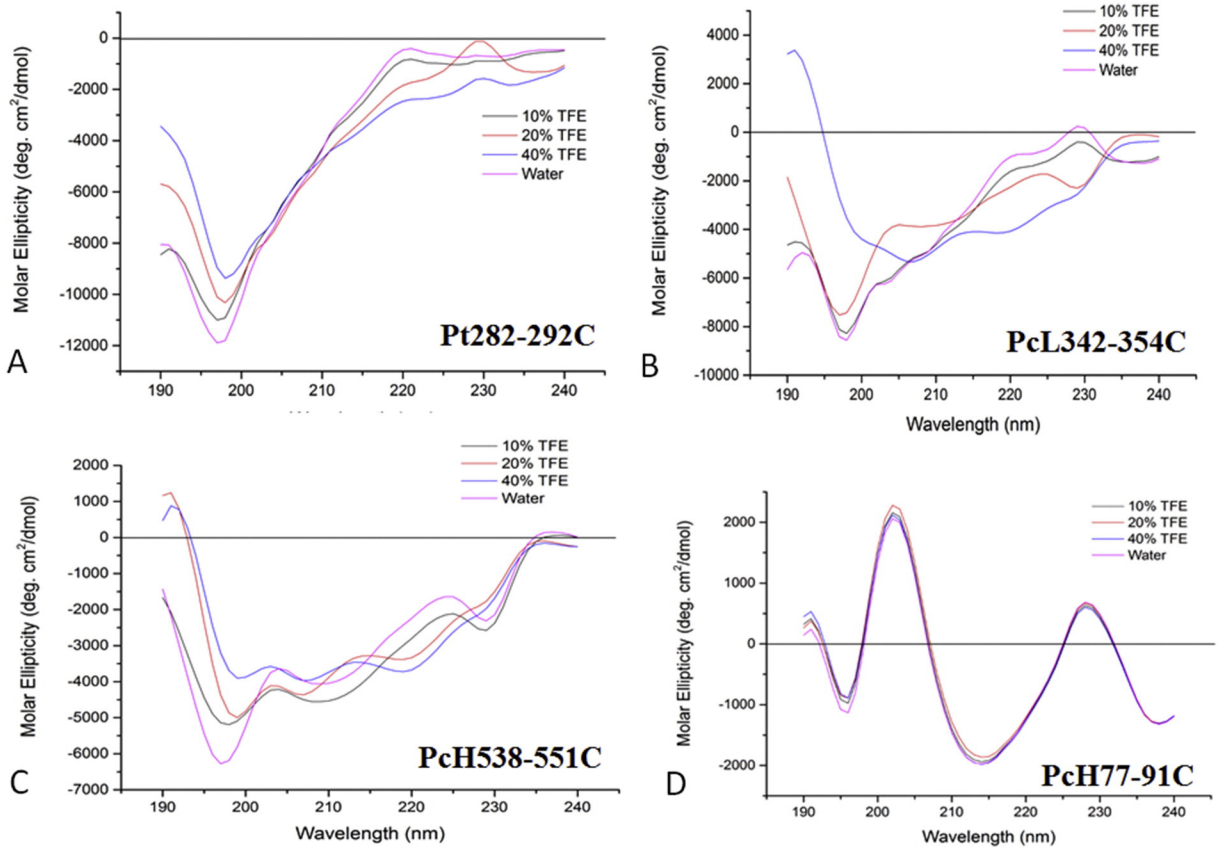

Fig. 3. Circular dichroism studies of peptides in aqueous solution and 10, 20, and 40% 2,2,2-trifluoroethanol. (A) Pt282-292C, (B) PcL342–354C, (C) PcH538-551C, and (D) PcH77-91C.

3.3. Electrochemistry characterization

3.3.1. PcL342–354C monolayer films

For a better understanding of the electrochemical response of PcL342–354C, the adsorption time of this peptide on ITO was tested (Fig. 4A) using a 0.05 mol·L^{-1} H_2SO_4 solution as the electrolyte. These conditions were chosen based on literature [26,43] that describes electrochemical studies of peptide Dermaseptin 01 using similar conditions. Fig. 4A shows the influence of adsorption time of PcL342–354C on the final response of the monolayer film obtained. Fig. 4B shows the results in another electrolytic medium (0.10 mol·L^{-1} PBS), which is one of the most biologically compatible buffers [44].

With increasing adsorption time, there was a corresponding increase in faradaic current density of the monolayer film of the peptide (Fig. 4A). The optimal time of 5 min is in accord with related studies [26,43]. Only 5 min of adsorption time is sufficient the peptide adsorb in electrode surface, thus enabling a good electrochemical response. For all adsorption times tested, PcL342–354C exhibited an irreversible oxidation process at +1.1 V vs. Ag/AgCl in the H_2SO_4 electrolyte.

Fig. 4B shows that the electrolyte employed in the electrochemical characterization of PcL342–354C, with the peptide monolayer obtained with 5 min of the adsorption time, has an important effect on the oxidation potential of this peptide. The process observed at +1.1 V vs. Ag/AgCl in the acidic medium shifted to lower potential values when employing PBS as the supporting electrolyte. In PBS (pH 7.2), the oxidation process was at +0.87 V, whereas in PBS (pH 8.0) it was at +0.83 V (Fig. 4B). It is noteworthy that in PBS (pH 7.2), the oxidation process of PcL342–354C appeared more defined. For this reason and because PBS (pH 7.2) is biologically compatible buffer [44], this electrolyte was used in the following studies.

Fig. 5 shows the results obtained from the investigation of the mechanism that governs the electrochemical response of PcL342–354C. Fig. 5A shows the cyclic voltammograms obtained for the peptide at different scan rates (v). Fig. 5B shows a linear relationship between the peak current (ip) of the oxidation process of PcL342–354C and the scan rate. This relationship indicates that the peptide is thermodynamically stabile under the experimental conditions employed [45]. This correlation also suggests that charge transfer at the electrode/electrolyte interface occurs in a regular manner and that the electrochemical processes are governed by charge transfer processes due to the ratio between ip and v had a correlation coefficient of $R^2 = 0.998$ [46,47]. These results also suggest that the peptide is strongly adsorbed on the electrode surface [48].

3.3.2. Bilayer films containing natural or synthetic polymers intercalated with PcL342–354C

Subsequently, we attempted to improve the electrochemical signal of PcL342–354C. Initially, we investigated the intercalation of this peptide with natural biopolymers, such as chitosan (cationic biopolymer), agar, and alginate (anionic biopolymer). Many studies in the literature, including those of our research group, have shown that natural polymers are excellent candidates for construction of sensor devices because these polymers improve the electrochemical stability of the system, promote better adsorption of the electroactive material, and allow control of the film thickness by the number of layers adsorbed [14,16,17,49,50]. Furthermore, these polysaccharides are inexpensive, abundant, easy to isolate and purify, and environmentally compatible [51].

Fig. 6 shows the electrochemical response of PcL342–354C after intercalation with chitosan (Fig. 6A), agar (Fig. 6B), and alginate (Fig. 6C) in the form of LbL films containing one or two bilayers. For comparison, the response of the monolayer film containing only the peptide is also shown.

Fig. 6A shows that chitosan reduces the electroactivity of the peptide. The current obtained for the ITO/chitosan/PcL342–354C film

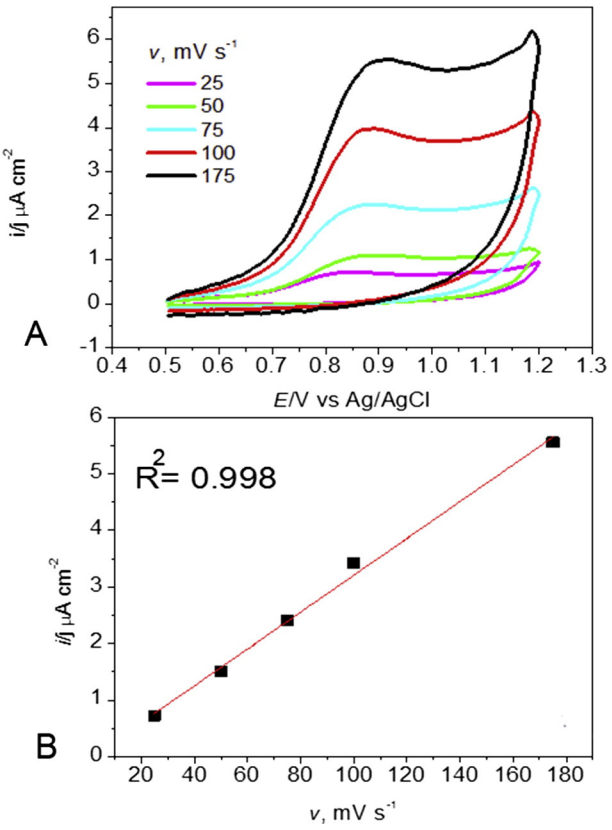

Fig. 5. (A) Influence of scan rate on the electrochemical response of PcL342–354C. (B) Linear correlation between the peak current of the oxidation process of PcL342–354C and the scan rate. All measurements were carried out in 0.1 mol·L^{-1} PBS (pH 7.2).

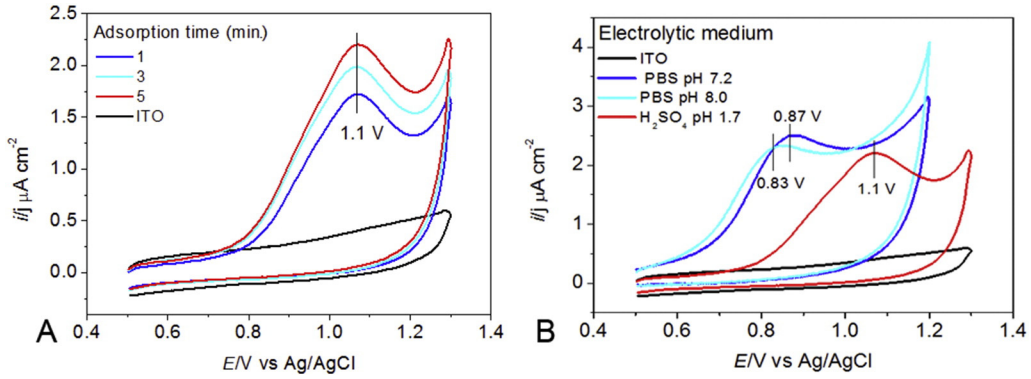

Fig. 4. (A) Influence of adsorption time of PcL342–354C on the ITO electrode in an electrolytic medium of 0.05 mol·L^{-1} H_2SO_4. (B) Influence of the electrolyte (0.05 mol·L^{-1} H_2SO_4 or 0.1 mol·L^{-1} PBS) on the response of PcL342–354C. All measurements were performed using a new modified electrode for every measurement (v = 50 mV·s^{-1}).

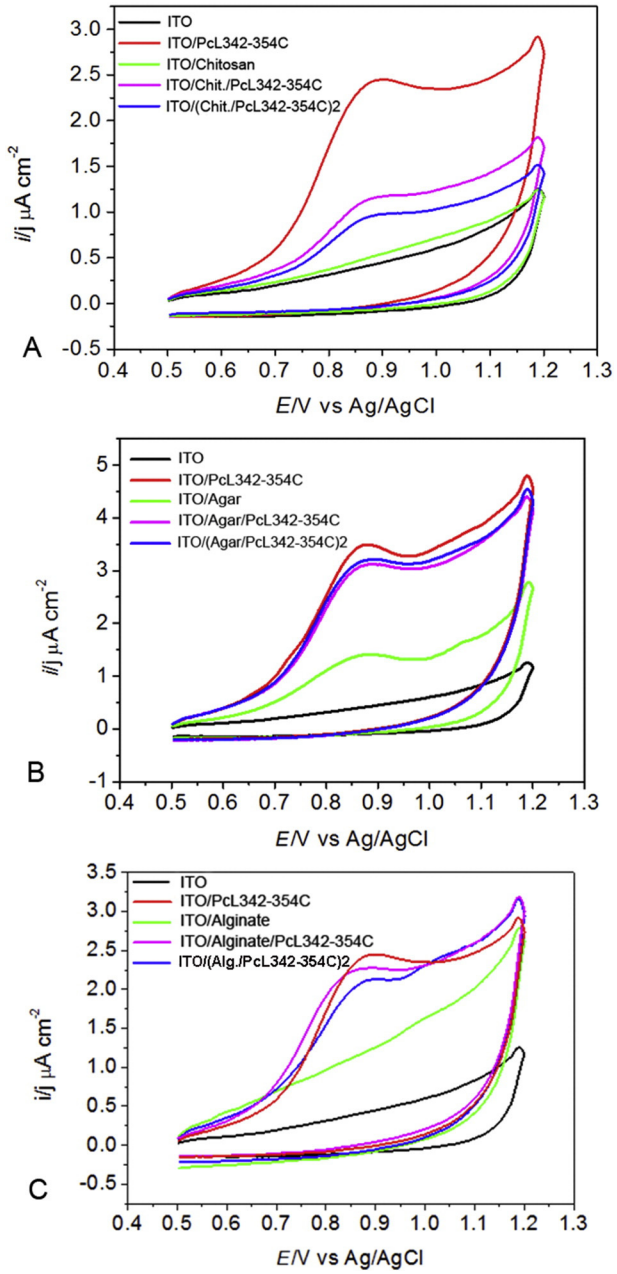

Fig. 6. Influence of (A) chitosan (chit.), (B) agar, or (C) alginate (alginate) and the number of bilayers on the electrochemical response of PcL342–354C. All measurements were carried out in 0.1 mol·L^{-1} PBS (pH 7.2), $v = 100$ mV·s^{-1}.

was lower than that obtained for the PcL342–354C monolayer film, and the current further decreased with increased numbers of bilayers on the film (ITO/(chitosan/PcL342–354C)$_2$). This behavior suggests that chitosan reduces the affinity of the peptide for the electrode, hindering charge transfer between the peptide and electrode/electrolyte interface. This is supported by the results showed in Fig. 6B and C with anionic polymers. PcL342–354 is a positively charged peptide (+1 net charge). Because of this, there was probably lower adsorption of PcL342–354C because of charge repulsion between chitosan and the peptide, resulting in its adsorption only through secondary interactions [52].

When agar or alginate (negative biopolymers; Fig. 6B and C, respectively) where used, the current density obtained for the bilayer films were similar to that recorded for the monolayer film containing only the peptide, even when the number of bilayers was increased. It is noteworthy that even without an improvement in the electrochemical response of PcL342–354C, when we used these seaweed polymers, the peptide response was not suppressed and remained at the same current level observed for the film containing only the peptide. Therefore, it is interesting to note that these films are biocompatible systems, containing a new peptide that is still little explored, which opens prospective studies for application of these films in other biotechnology areas.

In a further attempt to improve the electrochemical response of PcL342–354C, the peptide was intercalated with polymers widely used for this purpose, such as PEI and PSS [53–56]. Considering that PEI and PSS have, respectively, positive and negative charges, the film was adsorbed according to the electrostatic interaction mechanism [37]. PEI was used to give the substrate a positive charge for better adsorption of PSS, whereas PSS was used to increase the adsorption of PcL342–354C and consequently the electrochemical signal of the peptide.

Fig. 7 shows the response of the ITO/PEI/(PSS/PcL342–354C)$_n$ film containing one or two (n = 1 or 2) adsorbed bilayers. For comparative purposes, the responses of the film without the peptide and the film containing only the peptide are also shown. The ITO/PEI/PSS film did not show any redox process within the potential range investigated. On the other hand, when the peptide was adsorbed, an oxidation process was observed at +1.27 V, which can be directly assigned to the response of the peptide immobilized in the LbL bilayer structure containing PEI and PSS. In this case, the current observed was 100 times higher than that recorded for the peptide adsorbed directly on ITO (Fig. 7, inset). Furthermore, the joint presence of PEI and PSS increased the electrochemical stability of the adsorbed peptide, as a greater potential must be applied to achieve oxidation. Moreover, the oxidation process was observed for several consecutive cycles only when PEI and PSS were used. The system proposed here is very promising for future applications in GMO sensors; therefore, we undertook a more thorough characterization of this film.

3.4. Spectroscopic and diffractometric characterization

Absorption in the UV–Vis region allows the formation of an LbL film to be monitored because the absorbance that occurs at a characteristic wavelength for the absorbing molecules in the film is related to the thickness of the film (Beer–Lambert law), and indicates the continuity of the adsorption process in each adsorption stage [52]. In this sense, we studied the growth kinetics and formation of the ITO/PEI/(PSS/PcL342–354C)$_n$ film (Fig. 8A). PSS absorbs in the region near 300 nm [57] and was therefore chosen to monitor film formation. It should be noted that the peptide used in the film does not absorb significantly in the UV region because there are not aromatic amino acids in the sequence (e.g., tryptophan and tyrosine).

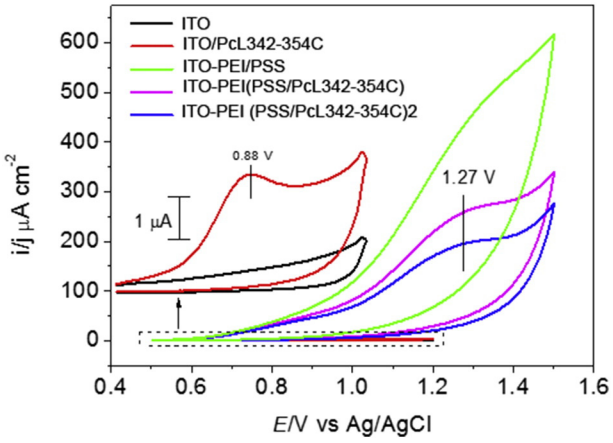

Fig. 7. Influence of ITO modified with a film of PEI/PSS and the number of bilayers of PSS/PcL342–354C on the electrochemical response of the film. The inset shows an expanded view of the response of the ITO/PcL342–354C film. All measurements were carried out in 0.1 mol·L^{-1} PBS (pH 7.2), $v = 100$ mV·s^{-1}.

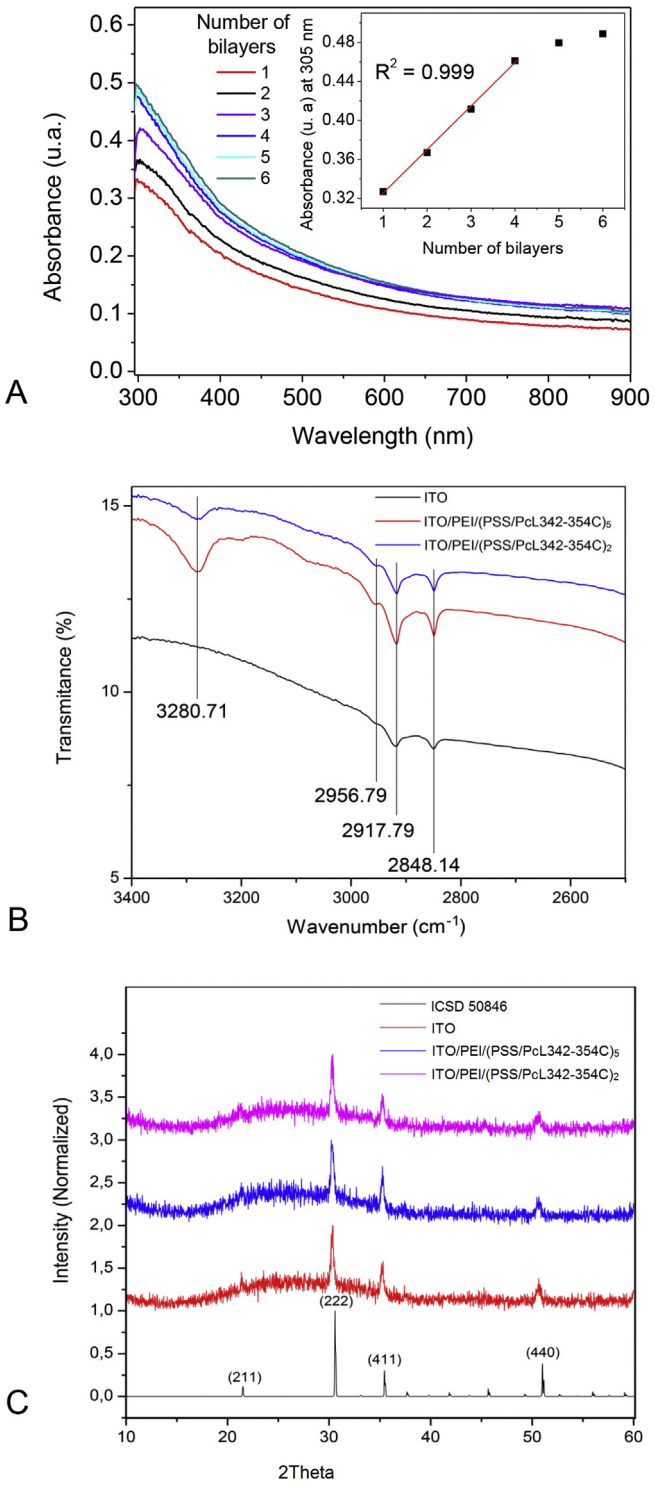

Fig. 8. (A) UV–Vis spectra showing the growth of the film with increasing numbers of bilayers (n) of ITO/PEI/(PSS/PcL342–354C)$_n$. The inset shows the relationship between the absorbance at 305 nm and the number of bilayers adsorbed. (B) FTIR spectra with characteristic bands identified. (C) XRD patterns with the main *hkl* indexes identified.

Fig. 8A shows the UV–Vis spectra recorded consecutively after the adsorption of each bilayer in ITO/PEI/(PSS/PcL342–354C)$_n$. The absorption increased linearly (Fig. 8, inset) to the fourth bilayer adsorbed. Apparently, five bilayers was saturated the system, leading to a change to a flatter slope, indicating the impossibility of adsorbing more than five bilayers. The FTIR spectra of these films are presented in Fig. 8B, and show O–H stretching vibrations at 3280 cm^{-1} and C–H stretching of the aliphatic chain at 3000–2800 cm^{-1}. In Fig. 8C, XRD diffractograms are shown, and we can conclude that the ITO film crystallizes in a cubic bixbyite structure (In_2O_3). The XRD method is a rapid analytical technique primarily used for phase identification of crystalline materials and can provide information on unit cell dimensions. The observed 2θ peaks are associated to the (211), (222), (411), and (440) planes, corresponding to inorganic crystal structure database (ICSD) file number 50,846 [58]. The high intensity of the (222) plane demonstrates the preferential growth direction of the ITO films and is dependent of the deposition conditions.

3.5. Atomic Force Microscopy

AFM was used to examine the morphology and quantify the surface roughness of the films produced. The ITO substrate was first studied as a control, and then the process of LbL film was examined to observe the effect of the number of bilayers adsorbed. Representative images are shown in Fig. 9. The microstructures observed for ITO are well-known features that have been previously observed by AFM [14,39]. The structures shown in Fig. 9A consist of flat "islands", each covering an area of 100 nm^2 to 1 μm^2 and consisting of small globular grains (<40 nm) that are above globular-like grains located on a lower level. The ITO/PEI film in Fig. 9B is very similar to that of ITO; however, this film has a smoother appearance, probably because the interstices between the flat "islands" are filled, as can be clearly seen in the 3D AFM images in the Supplementary material (Fig. S1). In the ITO/PEI/PSS film in Fig. 9C, the ITO structure was still visible, though very small granular additions (approximately 50 nm) started to be observed. On the other hand, after the adsorption of the peptide in the ITO/PEI/(PSS/PcL342–354C) film (Fig. 9D), the granular morphology of ITO was no longer observed, and the film showed a fibrous, uniform pattern. The immobilized peptide formed self-assembled nanofibers with diameters ranging from 100 to 200 nm, which is very similar to that described in AFM studies of other peptides [59]. The two-bilayer film of ITO/PEI/(PSS/PcL342–354C)$_2$ showed a similar morphology to that of the bilayer film, though it is apparent that a greater amount of peptide is adsorbed (Fig. 9E). In the five-bilayer film (Fig. 9F) further fibrous aspects are observed; however, the features are somewhat disguised, probably due to several interleaved layers of PSS/PcL342–354C, which corroborates the UV–Vis results, where it was difficult to absorb further bilayers. The roughness of the film surfaces was also studied. In Fig. 10, the average value of surface roughness and the calculated deviation for each sample are shown. AFM is essential for studying surface roughness (Ra or average deviation) on the nanoscale, with resolution far exceeding that of other stylus and optical based methods [60]. ITO had an average roughness of 2.2 ± 1.7 nm, which is very close to what has been reported elsewhere [14,39]. No significant differences were found ($p < 0.01$) between the roughness of ITO and that of the ITO/PEI and ITO/PEI/PSS films. However, ITO/PEI/PSS was significantly ($p < 0.01$) rougher when compared to ITO/PEI. All films containing the peptide had higher surface roughness than that of ITO. However, there was no difference between the surface roughnesses of the films with one, two, or five bilayers (Fig. 10) when compared at a 1% significance level. In general, all the films were soft and are ideal surfaces for biotechnological applications.

4. Conclusions

LbL films containing the PcL342–354C peptide derived from the protein Cry1Ab16 were successfully obtained through a simple and economical method. The isolated peptide showed electrochemical behavior similar to that of other peptides described in the literature. It was observed an irreversible oxidation process in electrolyte of 0.1 mol·L^{-1} potassium phosphate buffer (PBS) at pH 7.2. In addition, electrochemical response mechanism of the peptide was elucidated to be a purely adsorptive process. Among the natural polymers tested to optimize the electrochemical signal of PcL342–354C, chitosan proved impracticable, probably because of its positive charge. On the other hand, the negatively

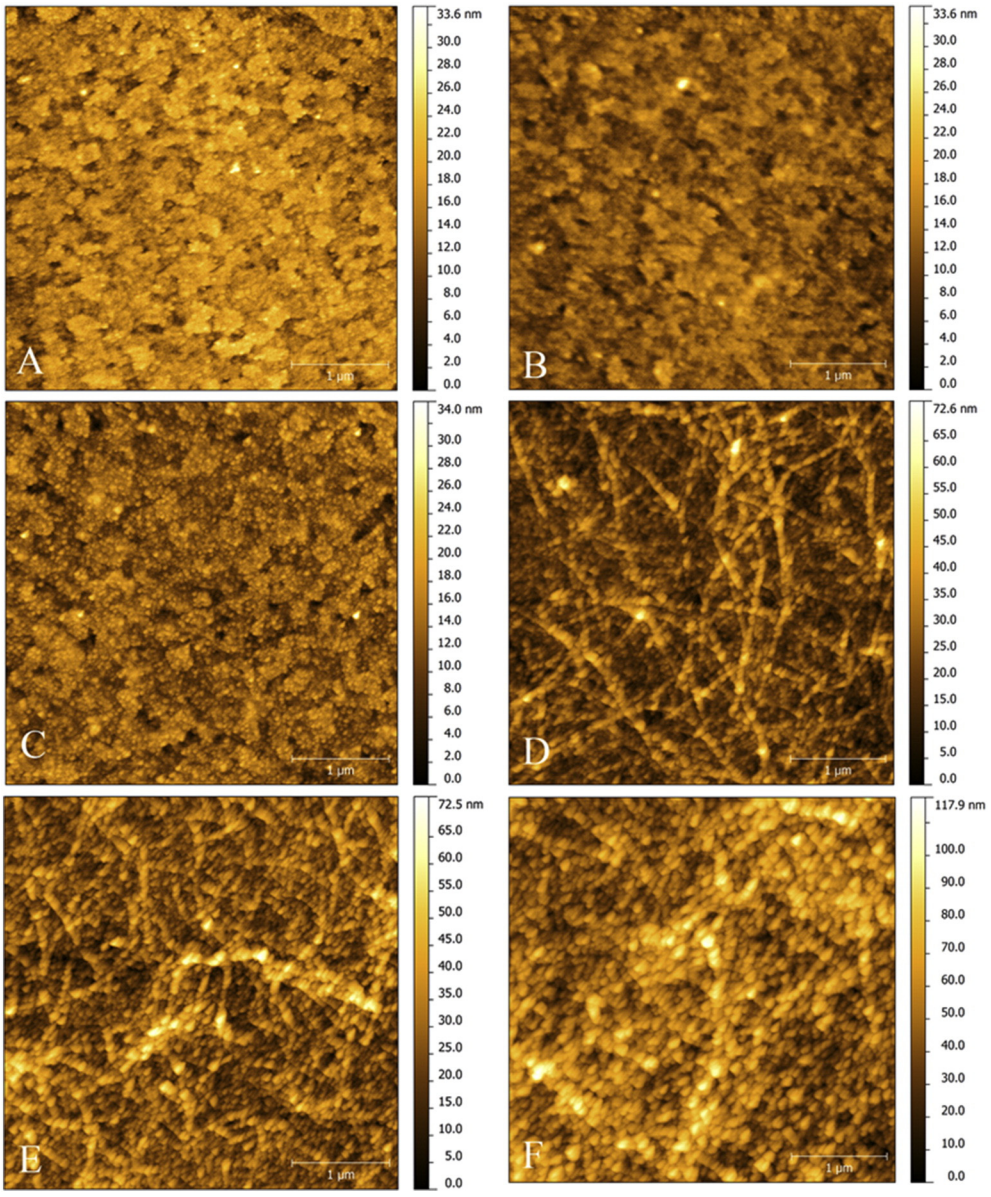

Fig. 9. Dynamic-mode AFM images of glass surfaces covered with (A) ITO, LbL films of (B) ITO/PEI, (C) ITO/PEI/PSS, (D) ITO/PEI/PSS/PcL342–354C, (E) ITO/PEI/$(PSS/PcL342–354C)_2$, and (F) ITO/PEI/$(PSS/PcL342–354C)_5$. All images are 4 × 4 μm in x and y.

charged natural polymers (agar and alginate) did not increase the signal of the peptide, but had no adverse effects. When combined in a multilayer structure, the synthetic polymers PEI and PSS surprisingly promoted an increase of the current density of the PcL342–354C process up to 100 times for ITO/PEI/(PSS/PcL342–354C). The AFM results showed that the adsorbed peptide formed self-assembled nanofibers with

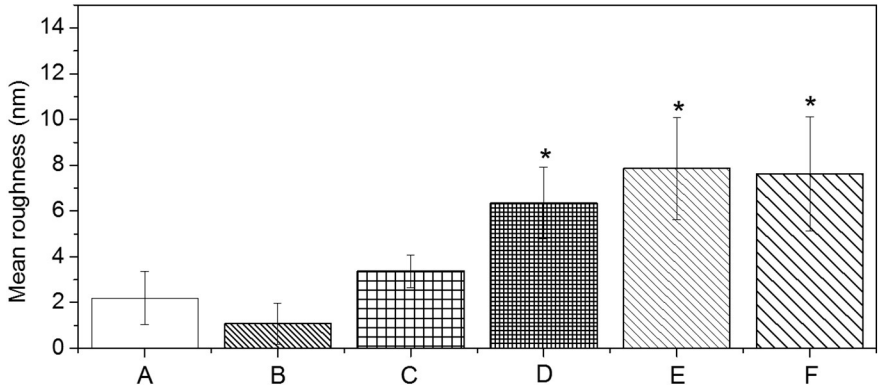

Fig. 10. Comparison of the Ra values of the surfaces of (A) ITO, (B) ITO/PEI, (C) ITO/PEI/PSS, (D) ITO/PEI/PSS/PcL342–354C, (E) ITO/PEI/$(PSS/PcL342–354C)_2$, and (F) ITO/PEI/$(PSS/PcL342–354C)_5$. *Statistically significant differences from ITO ($p < 0.01$).

diameters ranging from 100 to 200 nm on the polymeric film and very homogeneously distributed. UV–Vis spectra showed that the film increased linearly up to the fifth bilayer, after which this system reached saturation. The X-ray diffractograms revealed that the films contained an amorphous phase related to the peptides and diffraction peaks due to preferred orientation along the (222) direction of crystalline ITO. In general, the thorough characterization of the ITO/PEI/(PSS/PcL342–354C) film showed that this system is not only homogeneous and low cost, but is also reproducible, which opens prospects for future application of this film in electrochemical sensors for GMOs and environmental biosensors, among other biotechnological applications in the food safety area.

Acknowledgments

This work was partially supported by grants from the Brazilian funding agencies (Fundacao de Amparo a Pesquisa do Piaui) FAPEPI (Grant PI00045 PP SUS), (Comissão de Aperfeiçoamento de Pessoal do Nível Superior) CAPES (Grant 705/2009, *Nanobiomed* Network), and (Conselho Nacional de Desenvolvimento Científico e Tecnológico) CNPq (Grant 476700/2009-4). In addition, financial support was received from Consejo Nacional de Investigaciones Científicas y Técnicas (CONICET) (Grant PIP N°11220120100050CO) and Agencia Nacional de Promoción Científica y Tecnológica (ANPCyT) (Grant PICT N°1199). MMM is a researcher at CONICET. This work was also supported by Fundação para a Ciência e a Tecnologia (FCT) through grant number PEst-C/EQB/LA0006/2011. Alexandra Plácido is grateful to FCT for her grant SFRH/BD/97995/2013, financed by POPH–QREN–Tipologia 4.1–Formação Avançada, subsidized by Fundo Social Europeu and Ministério da Ciência, Tecnologia e Ensino Superior. ACM is indebted to FAPESP (Grant 2014/02282-6). YPM is grateful to CNPq (Grant 302674/2010-1).

Appendix A. Supplementary data

Supplementary data to this article can be found online at http://dx.doi.org/10.1016/j.msec.2016.01.011.

References

[1] Y. Taga, Recent progress of nanotechnologies of thin films for industrial applications, Mater. Sci. Eng. C 15 (2001) 231–235.
[2] N. Islam, K. Miyazaki, Nanotechnology innovation system: understanding hidden dynamics of nanoscience fusion trajectories, Technol. Forecast. Soc. Chang. 76 (2009) 128–140.
[3] S.D.F. Mihindukulasuriya, L.T. Lim, Nanotechnology development in food packaging: a review, Trends Food Sci. Technol. 40 (2014) 149–167.
[4] D.G. Castner, B.D. Ratner, Biomedical surface science: foundations to frontiers, Surf. Sci. 500 (2002) 28–60.
[5] M.S. Lord, M. Foss, F. Besenbacher, Influence of nanoscale surface topography on protein adsorption and cellular response, Nano Today 5 (2010) 66–78.
[6] P. Koegler, A. Clayton, H. Thissen, G.N.C. Santos, P. Kingshott, The influence of nanostructured materials on biointerfacial interactions, Adv. Drug Deliv. Rev. 64 (2012) 1820–1839.
[7] L.G. Paterno, L.H.C. Mattoso, O.N.d. Oliveira Jr., Filmes poliméricos ultrafinos produzidos pela técnica de automontagem: preparação, propriedades e aplicações, Quim. Nova 24 (2001) 228–235.
[8] J.O. Borges, J.F. Mano, Molecular interactions driving the layer-by-layer assembly of multilayers, Chem. Rev. 114 (2014) 8883–8942.
[9] M. Ferreira, P.A. Fiorito, O.N. Oliveira Jr., S.I. Córdoba de Torresi, Enzyme-mediated amperometric biosensors prepared with the Layer-by-Layer (LbL) adsorption technique, Biosens. Bioelectron. 19 (2004) 1611–1615.
[10] T.T.L. Souza, M.L. Moraes, M. Ferreira, Use of hemoglobin as alternative to peroxidases in cholesterol amperometric biosensors, Sensors Actuators B Chem. 178 (2013) 101–106.
[11] W. Huang, X. Li, Y. Xue, R. Huang, H. Deng, Z. Ma, Antibacterial multilayer films fabricated by LBL immobilizing lysozyme and HTCC on nanofibrous mats, Int. J. Biol. Macromol. 53 (2013) 26–31.
[12] Y. Nakane, I. Kubo, Layer-by-layer of liposomes and membrane protein as a recognition element of biosensor, Thin Solid Films 518 (2009) 678–681.
[13] Y. Wang, L. Hosta-Rigau, H. Lomas, F. Caruso, Nanostructured polymer assemblies formed at interfaces: applications from immobilization and encapsulation to stimuli-responsive release, Phys. Chem. Chem. Phys. 13 (2011) 4782–4801.
[14] E.A. de Oliveira Farias, M.C. dos Santos, N. de Araujo Dionísio, P.V. Quelemes, J.R.S.A. Leite, P. Eaton, D.A. da Silva, C. Eiras, Layer-by-Layer films based on biopolymers extracted from red seaweeds and polyaniline for applications in electrochemical sensors of chromium VI, Mater. Sci. Eng. B Solid 200 (2015) 9–21.
[15] P.R.S. Teixeira, A.S. do Nascimento Marreiro, E.A.O. Farias, N.A. Dionisio, E.C. Silva Filho, C. Eiras, Layer-by-layer hybrid films of phosphate cellulose and electroactive polymer as chromium (VI) sensors, J. Solid State Electrochem. (2015) 1–11.
[16] C. Eiras, A.C. Santos, M.F. Zampa, A.C.F. de Brito, C.J. Leopoldo Constantino, V. Zucolotto, J.R. dos Santos, Natural polysaccharides as active biomaterials in nanostructured films for sensing, J. Biomater. Sci. Polym. Ed. 21 (2010) 1533–1543.
[17] I. Araujo, M. Zampa, J. Moura, J. dos Santos, P. Eaton, V. Zucolotto, L. Veras, R. de Paula, J. Feitosa, J. Leite, Contribution of the cashew gum (*Anacardium occidentale* L.) for development of layer-by-layer films with potential application in nanobiomedical devices, Mater. Sci. Eng. C 32 (2012) 1588–1593.
[18] V. Ball, Organic and inorganic dyes in polyelectrolyte multilayer films, Materials 5 (2012) 2681–2704.
[19] P. Kongsuphol, S.K. Arya, C.C. Wong, L.J. Polla, M.K. Park, Coiled-coil peptide based sensor for ultra-sensitive thrombin detection, Biosens. Bioelectron. 55 (2014) 26–31.
[20] P. Thirupathi, L.N. Neupane, K.-H. Lee, Fluorescent peptide-based sensors for the ratiometric detection of nanomolar concentration of heparin in aqueous solutions and in serum, Anal. Chim. Acta 873 (2015) 88–98.
[21] X. Bai, B. Lu, X. Chen, B. Zhang, J. Tang, Reversible detection of vancomycin using peptide-functionalized cantilever array sensor, Biosens. Bioelectron. 62 (2014) 145–150.
[22] D. Pizzoni, M. Mascini, V. Lanzone, M. Del Carlo, C. Di Natale, D. Compagnone, Selection of peptide ligands for piezoelectric peptide based gas sensors arrays using a virtual screening approach, Biosens. Bioelectron. 52 (2014) 247–254.
[23] X. Wang, B. Piro, S. Reisberg, G. Anquetin, H. De Rocquigny, P. Jiang, Q. Wang, W. Wu, M.-C. Pham, C.-Z. Dong, Direct, reagentless electrochemical detection of the BIR3 domain of X-linked inhibitor of apoptosis protein using a peptide-based conducting polymer sensor, Biosens. Bioelectron. 61 (2014) 57–62.
[24] W. Zhou, B.P. Duckworth, R.J. Geraghty, Fluorescent peptide sensors for tyrosylprotein sulfotransferase activity, Anal. Biochem. 461 (2014) 1–6.
[25] A.J. Zaitouna, A.J. Maben, R.Y. Lai, Incorporation of extra amino acids in peptide recognition probe to improve specificity and selectivity of an electrochemical peptide-based sensor, Anal. Chim. Acta 886 (2015) 157–164.
[26] M.F. Zampa, I.M. Araújo, V. Costa, C.H.N. Costa, J.R. Santos, V. Zucolotto, C. Eiras, J.R.S. Leite, Leishmanicidal activity and immobilization of dermaseptin 01 antimicrobial peptides in ultrathin films for nanomedicine applications, Nanomedicine 5 (2009) 352–358.
[27] A. Plácido, J.S. Amaral, J. Costa, T.J.R. Fernandes, M.B.P.P. Oliveira, C. Delerue-Matos, I. Mafra, Novel strategies for genetically modified organism detection, in: E.I. Academic Press (Ed.), Genetically Modified Organisms in Food Production — Safety, Regulation and Public Health, Waltham, MA, USA 2016, pp. 119–131.
[28] M.M. Marani, J. Costa, I. Mafra, M.B.P. Oliveira, S.A. Camperi, J.R.S.A. Leite, In silico peptide prediction for antibody generation to recognize 5-enolpyruvylshikimate-3-phosphate synthase (EPSPS) in genetically modified organisms, Pept. Sci. 104 (2015) 91–100.
[29] A. Aris, S. Leblanc, Maternal and fetal exposure to pesticides associated to genetically modified foods in Eastern Townships of Quebec, Canada, Reprod. Toxicol. 31 (2011) 528–533.
[30] K. Carstens, J. Anderson, P. Bachman, A. De Schrijver, G. Dively, B. Federici, M. Hamer, M. Gielkens, P. Jensen, W. Lamp, Genetically modified crops and aquatic ecosystems: considerations for environmental risk assessment and non-target organism testing, Transgenic Res. 21 (2012) 813–842.
[31] R.B. Merrifield, Solid phase peptide synthesis. I. The synthesis of a tetrapeptide, J. Am. Chem. Soc. 85 (1963) 2149–2154.
[32] P. Wolf, A critical reappraisal of Waddell's technique for ultraviolet spectrophotometric protein estimation, Anal. Biochem. 129 (1983) 145–155.
[33] M.M. Marani, F.v.S. Dourado, P.V. Quelemes, A.R. de Araujo, M.r.L.G. Perfeito, E.A. Barbosa, L.M.C. Véras, A.L.R. Coelho, E.B. Andrade, P. Eaton, Characterization and biological activities of ocellatin peptides from the skin secretion of the frog *Leptodactylus pustulatus*, J. Nat. Prod. 78 (2015) 1495–1504.
[34] S.W. Provencher, J. Gloeckner, Estimation of globular protein secondary structure from circular dichroism, Biochemistry 20 (1981) 33–37.
[35] N. Sreerama, R.W. Woody, A self-consistent method for the analysis of protein secondary structure from circular dichroism, Anal. Biochem. 209 (1993) 32–44.
[36] W.C. Johnson, Analyzing protein circular dichroism spectra for accurate secondary structures, Proteins 35 (1999) 307–312.
[37] G. Decher, Fuzzy nanoassemblies: toward layered polymeric multicomposites, Science 277 (1997) 1232–1237.
[38] W. Kern, Purifying Si and SiO_2 surfaces with hydrogen peroxide, Semicond. Int. 7 (1984) 94–99.
[39] P. Eaton, P. West, Atomic Force Microscopy, Oxford University Press Inc., USA, 2010.
[40] J.M. Walker, The Proteomics Protocols Handbook, Springer, 2005.
[41] Y. Huang, L. He, G. Li, N. Zhai, H. Jiang, Y. Chen, Role of helicity of α-helical antimicrobial peptides to improve specificity, Protein Cell 5 (2014) 631–642.
[42] D.L. Lee, C.T. Mant, R.S. Hodges, A novel method to measure self-association of small amphipathic molecules temperature profiling in reversed-phase chromatography, J. Biol. Chem. 278 (2003) 22918–22927.
[43] M.F. Zampa, I.M.d.S. Araújo, J.R. Dos Santos Júnior, V. Zucolotto, J.R.S.A. Leite, C. Eiras, Development of a novel biosensor using cationic antimicrobial peptide and nickel phthalocyanine ultrathin films for electrochemical detection of dopamine, Int. J. Anal. Chem. 2012 (2012).
[44] C. Mohan, Buffers: A Guide for the Preparation and use of Buffers in Biological Systems, 2006.

[45] F.M. Kelly, J.H. Johnston, T. Borrmann, M.J. Richardson, Functionalised hybrid materials of conducting polymers with individual fibres of cellulose, Eur. J. Inorg. Chem. 2007 (2007) 5571–5577.
[46] X. Xie, T. Gan, D. Sun, K. Wu, Application of multi-walled carbon nanotubes/nafion composite film in electrochemical determination of Pb^{2+}, Fullerenes, Nanotubes, Carbon Nanostruct. 16 (2008) 103–113.
[47] S. Pruneanu, E. Veress, I. Marian, L. Oniciu, Characterization of polyaniline by cyclic voltammetry and UV–Vis absorption spectroscopy, J. Mater. Sci. 34 (1999) 2733–2739.
[48] A.J. Bard, L.R. Faulkner, Fundamentals and Applications, Electrochemical Methods, second ed. Wiley, New York, 2001.
[49] J.R.T. da Silva, E.A.D. Farias, E.C. Silva, C. Eiras, Development and characterization of composites based on polyaniline and modified microcrystalline cellulose with anhydride maleic as platforms for electrochemical trials, Colloid Polym. Sci. 293 (2015) 1049–1058.
[50] S.B.A. Barros, C.M.S. Leite, A.C.F. de Brito, J.R. Dos Santos Júnior, V. Zucolotto, C. Eiras, Multilayer films electrodes consisted of cashew gum and polyaniline assembled by the layer-by-layer technique: electrochemical characterization and its use for dopamine determination, Int. J. Anal. Chem. 2012 (2012).
[51] S.-K. Kim, Marine Cosmeceuticals: Trends and Prospects, CRC Press, 2012.
[52] E.A.O. Farias, N.A. Dionisio, P.V. Quelemes, S.H. Leal, J.M.E. Matos, E.C. Silva Filho, I.H. Bechtold, J.R.S. Leite, C. Eiras, Development and characterization of multilayer films of polyaniline, titanium dioxide and CTAB for potential antimicrobial applications, Mater. Sci. Eng. C 35 (2014) 449–454.
[53] J.L. DeLuca, D.P. Hickey, D.A. Bamper, D.T. Glatzhofer, M.B. Johnson, D.W. Schmidtke, Layer-by-layer assembly of ferrocene-modified linear polyethylenimine redox polymer films, ChemPhysChem 14 (2013) 2149–2158.
[54] K.R. Knowles, C.C. Hanson, A.L. Fogel, B. Warhol, D.A. Rider, Layer-by-layer assembled multilayers of polyethylenimine-stabilized platinum nanoparticles and PEDOT: PSS as anodes for the methanol oxidation reaction, ACS Appl. Mater. Interfaces 4 (2012) 3575–3583.
[55] J. Luo, Y. Chen, Q. Ma, R. Liu, X. Liu, Layer-by-layer self-assembled hybrid multilayer films based on poly(sodium 4-styrenesulfonate) stabilized graphene with polyaniline and their electrochemical sensing properties, RSC Adv. 3 (2013) 17866–17873.
[56] Z. Hu, J. Xu, Y. Tian, R. Peng, Y. Xian, Q. Ran, L. Jin, Layer-by-layer assembly of poly(sodium 4-styrenesulfonate) wrapped multiwalled carbon nanotubes with polyaniline nanofibers and its electrochemistry, Carbon 48 (2010) 3729–3736.
[57] S. Stankovich, R.D. Piner, X. Chen, N. Wu, S.T. Nguyen, R.S. Ruoff, Stable aqueous dispersions of graphitic nanoplatelets via the reduction of exfoliated graphite oxide in the presence of poly (sodium 4-styrenesulfonate), J. Mater. Chem. 16 (2006) 155–158.
[58] N. Nadaud, N. Lequeux, M. Nanot, J. Jove, T. Roisnel, Structural studies of tin-doped indium oxide (ITO) and In 4 Sn 3 O 12, J. Solid State Chem. 135 (1998) 140–148.
[59] T. Wang, X. Zhong, S. Wang, F. Lv, X. Zhao, Molecular mechanisms of RADA16-1 peptide on fast stop bleeding in rat models, Int. J. Mol. Sci. 13 (2012) 15279–15290.
[60] B. Bhushan, Modern Tribology Handbook, Principles of Tribology, 1, CRC Press, 2001.
[61] S. Kashyap, Computational modeling deduced three dimensional structure of Cry1Ab16 toxin from *Bacillus thuringiensis* AC11, Indian J. Microbiol. 52 (2012) 263–269.
[62] B. Bjellqvist, G.J. Hughes, C. Pasquali, N. Paquet, F. Ravier, J.C. Sanchez, S. Frutiger, D. Hochstrasser, The focusing positions of polypeptides in immobilized ph gradients can be predicted from their amino-acid-sequences, Electrophoresis 14 (1993) 1023–1031.
[63] J. Kyte, R.F. Doolittle, A simple method for displaying the hydropathic character of a protein, J. Mol. Biol. 157 (1982) 105–132.